Energy Storage Devices Hot Paper

DOI: 10.1002/anie.201409366

Flexible and Stretchable Lithium-Ion Batteries and Supercapacitors Based on Electrically Conducting Carbon Nanotube Fiber Springs**

*Ye Zhang, Wenyu Bai, Xunliang Cheng, Jing Ren, Wei Weng, Peining Chen, Xin Fang, Zhitao Zhang, and Huisheng Peng**

Abstract: *The construction of lightweight, flexible and stretchable power systems for modern electronic devices without using elastic polymer substrates is critical but remains challenging. We have developed a new and general strategy to produce both freestanding, stretchable, and flexible supercapacitors and lithium-ion batteries with remarkable electrochemical properties by designing novel carbon nanotube fiber springs as electrodes. These springlike electrodes can be stretched by over 300%. In addition, the supercapacitors and lithium-ion batteries have a flexible fiber shape that enables promising applications in electronic textiles.*

Flexible and stretchable electronic devices have emerged as an important branch of modern electronics.[1–7] They have found a wide variety of promising applications including smart clothes, electronic skins, stretchable displays, and flexible phones.[8–10] As a result, there is a need to develop corresponding power systems such as supercapacitors and lithium-ion batteries that should also be lightweight, flexible, and stretchable.[11–13] Conventional supercapacitors and lithium-ion batteries are typically rigid and heavy, and thus cannot meet the above requirements. Recently, some attempts have been made to fabricate stretchable supercapacitors and lithium-ion batteries, mostly by using elastomeric polymers such as polydimethylsiloxane or rubber as substrates to achieve stretchability.[14–19] However, this method has several problems: the introduction of noncapacitive elastomeric polymers increases the volume and weight of the device, which is not suitable for application in portable and wearable electronics; the device shows low specific capacitance and energy density when all the components are taken into account; the poor mechanical properties and low operating temperature of the elastomeric polymers also make them unstable during use.

[*] Y. Zhang, W. Bai, Dr. X. Cheng, J. Ren, Dr. W. Weng, P. Chen, X. Fang, Z. Zhang, Prof. H. Peng
State Key Laboratory of Molecular Engineering of Polymers
Department of Macromolecular Science and Laboratory of Advanced Materials, Fudan University
Shanghai 200438 (China)
E-mail: penghs@fudan.edu.cn

[**] This work was supported by MOST (2011CB932503), NSFC (21225417), STCSM (12nm0503200), the Fok Ying Tong Education Foundation, the Program for Special Appointments of Professors at Shanghai Institutions of Higher Learning, and the Program for Outstanding Young Scholars from the Organization Department of the CPC Central Committee.

Supporting information for this article is available on the WWW under http://dx.doi.org/10.1002/anie.201409366.

We report herein a new and general strategy for the fabrication of freestanding (i.e., no substrate is required) elastic supercapacitors and lithium-ion batteries with high electrochemical performances by using fiber springs as electrodes. The springlike fiber electrodes comprised twisted aligned multiwalled carbon nanotubes (CNTs) with uniform coiled loops, which provided the electrode with a high stretchability and elongation of over 300%. An elastic supercapacitor was fabricated by placing two springlike fibers in parallel, while an elastic lithium-ion battery was produced from two springlike fibers bearing $LiMn_2O_4$ (LMO) and $Li_4Ti_5O_{12}$ (LTO) nanoparticles as positive and negative electrodes. Both the fiber-shaped supercapacitors and lithium-ion batteries were lightweight (linear density of 10^{-2}–10^{-1} mg cm^{-1}), flexible, and stretchable, and their electrochemical performance was maintained during bending and stretching deformations.

Spinnable CNT arrays were first synthesized by chemical vapor deposition,[20,21] and aligned CNT sheets were then pulled out of the CNT array, followed by spinning into CNT fibers. The CNT fiber had a diameter of approximately 12 μm (Figure S1 in the Supporting Information). The springlike fiber was prepared by overtwisting several CNT fibers together,[22,23] of which the diameter was dictated by the number of CNT fibers (Figure S2). Figure 1a,b shows a typical fiber overtwisted from ten CNT fibers with coiled loops aligning along the fiber axis. The fiber was highly flexible and lightweight with a linear density of 0.033 mg cm^{-1}, which was measured by a microbalance with resolution of 0.1 μg. Figure 1c shows that the CNTs were highly aligned along the helical direction in the coiled loops, which had approximate diameters of 65 μm and pitch distances of 30 μm that gave the fiber elasticity. It can be easily stretched and released up to 100%, as shown in Figure 1d–f. The coiled loops were gradually elongated with the CNTs remaining highly aligned during stretching, and the springlike fiber returned to the original coiled structure after release.

The aligned structure of CNTs means that the springlike fiber exhibits excellent electronic and mechanical properties. For instance, the fiber has a high electrical conductivity on the level of 10^2–10^3 S cm^{-1}, thus making it useable as an electrode. For an elastic conducting fiber, the stretchability can be further quantitatively investigated by tracing the electrical resistances during the stretching and releasing processes. As shown in Figure 1g, the initial resistance of the springlike fiber was 0.19 kΩ cm^{-1}, and the resistances slightly increased to 0.25 kΩ cm^{-1} with tensile strains up to 100%. The resistance then recovered to 0.20 kΩ cm^{-1} after release. The mechanical properties of the fiber were also characterized by

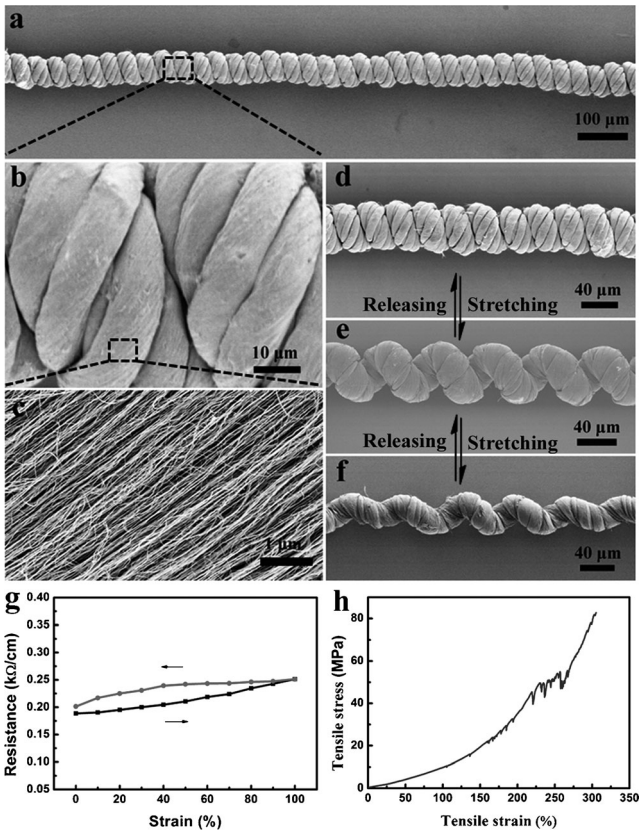

Figure 1. a–c) Scanning electron microscopy (SEM) images of a springlike fiber at different magnifications. d–f) SEM images of a fiber at different strains 0% (d) 50% (e), and 100% (f). g) Evolution of resistances of the fiber during a stretching and releasing process with a strain of 100%. h) Tensile stress–strain curve of a fiber.

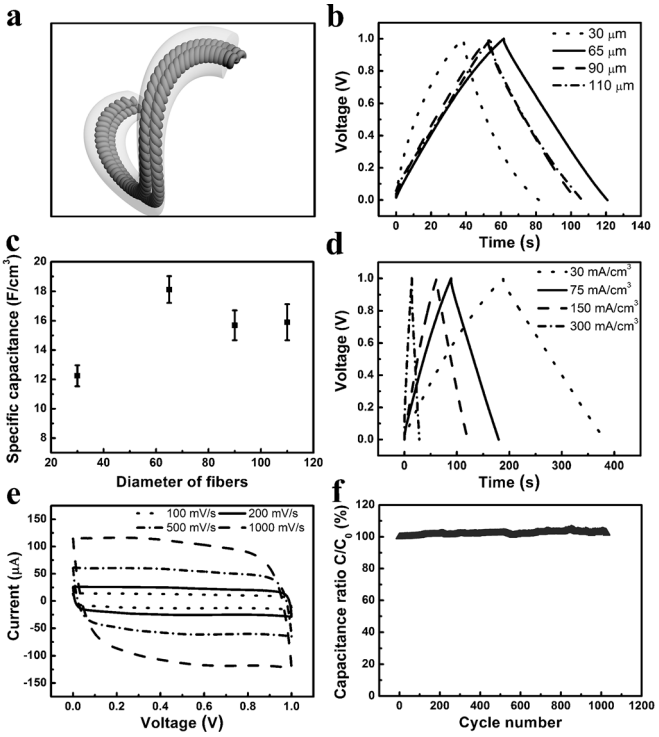

Figure 2. Electrochemical performance of a fiber-shaped supercapacitor. a) Structure of the supercapacitor. b) Galvanostatic charge–discharge curves of fibers with different diameters at a current density of 150 mA cm^{-3}. c) Dependence of specific capacitance on the fibre diameter. d) Galvanostatic charge–discharge curves at different current densities. e) Cyclic voltammogram (CV) curves at different scan rates. f) Cyclic performance of the supercapacitor. C_0 and C correspond to specific capacitances at the initial and subsequent cycles, respectively. The fiber diameter is 65 μm in (d)–(f).

the stress–strain curve (Figure 1h). As expected, the fiber showed a high elongation of 305% with an ultimate tensile stress of 82.7 MPa. If the tensile strain were below 100%, the relation of tensile stress (σ) and strain (ε) obeys Hooke's law: $\sigma = E\varepsilon$. The elasticity modulus (E) was 9.80 MPa, which is comparable to rubber.

To fabricate an elastic fiber-shaped supercapacitor, the springlike fiber was first coated with the PVA/H_3PO_4 gel electrolyte (Figure S3 in the Supporting Information), which also functioned as the separator to prevent short circuits. The symmetric device was made from two fibers, which exerted a significant impact on the performance (Figure 2a). We first compared the electrochemical performances of fibers with different diameters controlled by the number of CNT fibers, namely 30, 65, 90, and 110 μm from 5, 10, 15, and 20 CNT fibers, respectively. The cyclic voltammograms of the supercapacitors with different diameters at a scan rate of 20 mV s^{-1} are shown in Figure S4. A typical rectangular shape was observed for all supercapacitors, thus indicating an electrical double-layer behavior.[16,24] Galvanostatic charge–discharge curves between 0 and 1 V at a current density of 150 mA cm^{-3} are shown in Figure 2b. The symmetric triangular shapes suggest a high reversibility and Coulombic efficiency during the charge and discharge processes. The charge–discharge time, which shows the capacitance, first increased with diameter from 30 to 65 μm, and then decreased with larger diameter. The specific capacitances as a function of volume of the fiber electrodes are shown in Figure 2c. Consistent with the results shown in the galvanostatic charge–discharge curves, the specific capacitances increased with electrode diameters from 12.25–18.12 F cm^{-3} in the range 30–65 μm because of the reduced electrical resistance (Figure S5). The resistance slightly decreased to 15.59 F cm^{-3} when the diameter further increased to 110 μm as permeation of the gel electrolyte into the fiber electrode becomes difficult. In this case, an optimal diameter occurred at 65 μm for the fiber-shaped supercapacitor and was used in the following discussion unless otherwise specified.

The rate performances, which show the electrochemical behavior under different current densities, are given in Figure 2d. The charge–discharge curves retained the symmetrical triangular shape from 30–300 mA cm^{-3}, thus suggesting that the supercapacitors can perform stably over a wide range of current densities. CV curves with increasing scan rates from 100 to 1000 mV s^{-1} are shown in Figure 2e, and the specific capacitances calculated based on the CV curves are shown in Figure S6. The rectangular shapes and the specific capacitances varied slightly with the increasing scan rate, thus indicating a high electrochemical performance during the rapid charge–discharge process. In addition, the supercapacitor exhibited a high stability as exemplified by the well-maintained specific capacitance after 1000 cycles (Figure 2f).

The supercapacitors showed energy densities up to 0.629 mWh cm^{-3} and power densities up to 37.74 mW cm^{-3}. To clarify the performance of the fiber-shaped device, the specific capacitance can be also converted to 0.51 mF cm^{-1} and 27.07 mF cm^{-2} on the basis of the length and the area of the electrode at 150 mA cm^{-3}. Note that nonstretchable fiber-shaped supercapacitors from carbon-based electrodes were previously reproted but with much lower specific capacitances, such as 0.006 mF cm^{-1} for a bare CNT fiber, 0.014 mF cm^{-1} for a CNT/MnO_2 hybrid fiber, and 11.9–19.5 mF cm^{-2} for a pen ink electrode.[25–26] The excellent electrochemical performance of the supercapacitor was attributed to the hierarchical helical structure of the aligned CNTs, which significantly increased the surface area of electrode per unit length.

The superapacitor is flexible and stretchable. It can be bent in any direction without degradation in performance, as verified by the identical curves shown in Figure 3a. The specific capacitance remained at 93.5% after 300 bending cycles (Figure 3b). When the supercapacitor was stretched to 100%, the CV curves remained unchanged and the specific capacitance remained above 90% (Figure 3c,d). The supercapacitor was further tested under long-term repeated stretching, and more than 94% of the specific capacitance remained after 300 stretching cycles (Figure 3e). In the stretched state, the supercapacitor also performed stably over 1000 cycles, thus indicating a remarkable resistance against deformation.

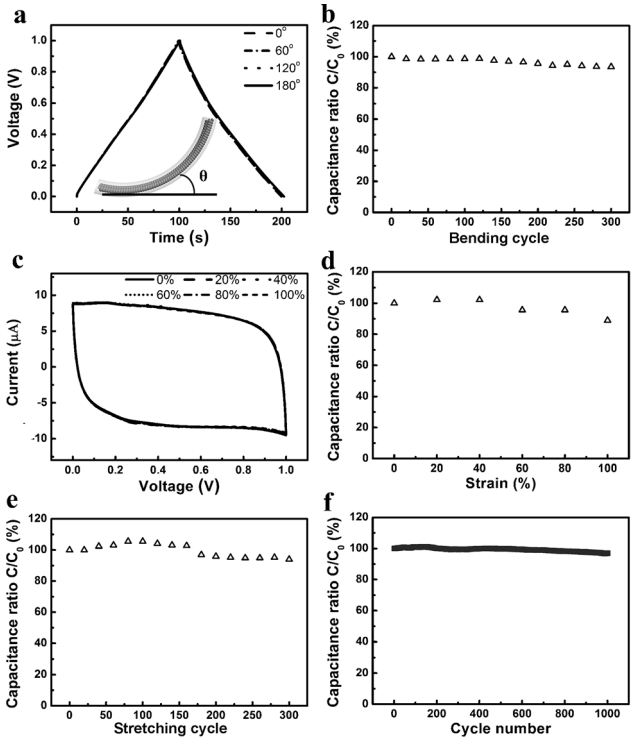

Figure 3. a) Galvanostatic charge–discharge curves of a supercapacitor bent to different angles. b) Evolution of specific capacitance over bending times at a bending angle of 180°. c) CV curves of a supercapacitor with increasing strains to 100%. d, e) Evolutions of specific capacitance over strain and number of stretching cycles at a strain of 100%, respectively. f) Cyclic performance of a 100% stretched supercapacitor.

Similar to reported stretchable supercapacitors based on elastomeric polymer substrates,[16,17,27–29] our supercapacitor could be stretched by 100%. However, the electrochemical properties, such as specific capacitances, of the reported elastomeric substrate-based stretchable supercapacitors were calculated only from the active materials without considering the large and heavy substrate, which is not effective for practical applications.[30] The specific capacitances would be much lower after the substrate was included. For instance, a stretchable fiber-shaped supercapacitor has been reported to have a specific volume capacitance of 10.9 mF cm^{-3} based on the whole device, which was fabricated by winding a CNT sheet on an elastic fiber.[16] In contrast, our substrate-free elastic supercapacitor displays a much higher specific capacitance of 1587 mF cm^{-3}, over 145 times that of the one based on an elastic substrate under the same conditions.

The springlike fiber, which provides adequate space accessible for functional guests, can not only be used in fiber-shaped supercapacitors, but is also applicable in lithium-ion batteries. We demonstrated that after the introduction of active nanoparticles, the resulting hybrid springlike fiber can serve as electrodes for fiber-shaped lithium-ion batteries. LTO and LMO nanoparticles were incorporated into the CNT fibers to prepare CNT/LTO and CNT/LMO hybrid fibers, respectively (see the Experimental Section).[31,32] Both LTO and LMO aggregates were irregular in morphology with sizes of 80–210 nm and 50–170 nm, respectively (Figure S7 and S8). Both LTO and LMO nanoparticles exhibited spinel phases that were confirmed by X-ray diffraction patterns (Figure S9 and S10).[33] The CNT/LTO and CNT/LMO fibers were prepared by immersing the CNT sheet into LTO and LMO suspensions, followed by rolling into fibers. The LTO and LMO contents in the hybrid fibers were controlled by varying the concentrations of the suspensions. For instance, the LTO weight percentages were increased from 21% to 47% and to 65% with increasing LTO concentrations from 0.5 to 1 and to 5 mg mL^{-1}, respectively; the LMO weight percentages were increased from 30% to 56% and to 86% with increasing LMO concentrations from 0.5 to 1 and to 5 mg mL^{-1}, respectively. Likewise, the CNT hybrid fiber was the building block for hierarchical springlike architecture. For example, ten CNT/LTO fibers and CNT/LMO fibers were overtwisted into springlike hybrid fibers. After being impregnated with the gel electrolyte that also served as the separator, the CNT/LTO and CNT/LMO fibers were encased to produce a fiber-shaped lithium-ion battery, and the maximum LTO and LMO content of the hybrid fiber was used in the following discussion if not specified.

Figure 4a shows the CNT/LTO fiber where CNTs acted as conducting scaffolds and the LTO nanoparticles were well-dispersed among them (Figure 4b,c). Similarly, the LMO nanoparticles were also uniformly dispersed in the CNT/LMO hybrid fiber (Figure S11 in the Supporting Information). The linear densities were 0.094 mg cm^{-1} and 0.235 mg cm^{-1} for the CNT/LTO fiber and CNT/LMO fiber, respectively. The aligned CNTs served as scaffolds and current collectors to ensure effective charge transport. Compared with traditional batteries, no binder, conducting

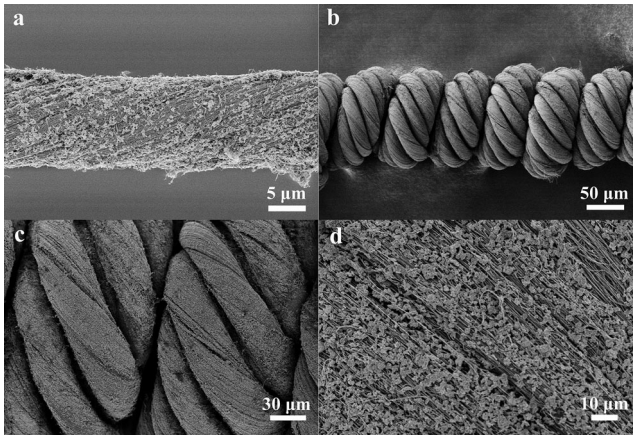

Figure 4. a) SEM image of a CNT/LTO hybrid fiber. b–d) SEM image of a CNT/LTO hybrid fiber at different magnifications.

diluents, and metal current collector were required, which drastically reduced the weight of the battery.

The electrochemical performances of the CNT/LTO and CNT/LMO electrodes were first tested in half cells with Li wires as the counterelectrode. Typical charge and discharge curves for the CNT/LTO electrode displayed an average discharge plateau at 1.5 V and a specific capacity of 145.9 mAh g^{-1} at 0.1 mA cm^{-1} (Figure S12a in the Supporting Information). The specific capacity was based on the total weight of the fiber electrode, including both LTO and CNTs. After 100 charge–discharge cycles, the capacities remained at 91.8%, thus indicating a good cyclic stability (Figure S12a). For the CNT/LMO electrode, two characteristic charge plateaus were observed at 4.0 and 4.2 V. The specific capacities was 72.5 mAh g^{-1} at the first cycle and remained by 86.8% after 100 cycles at 0.1 mA cm^{-1}. The CNT/LTO showed better capacity retention becuase of the better structural stability during the lithiation and delithiation processes. To construct the full battery, the CNT/LTO electrode was used as the anode (negative electrode) that determined the capacity of the entire battery, while the CNT/LMO electrode was the cathode (positive electrode) that had a capacity around 1.5 times that of the anode.[33,34]

Figure 5a shows the typical charge–discharge profile of the full fiber-shaped battery at 0.1 mA cm^{-1}. The average discharge voltage plateau of 2.5 V was consistent with the potential difference between the CNT/LTO and CNT/LMO electrodes. The battery exhibited a reversible capacity of 2.2 mAh m^{-1} based on the length of the battery and 92.4 mAh g^{-1} based on the mass of the CNT/LTO electrode; this result is consistent with previously reported planar batteries.[33–35] The capacity remained at 92.1% after running for 100 cycles. The battery was also highly stretchable, and the capacity remained at 85% at 100% strain (Figure 6a). In addition, the capacity varied within less than 1% after repeated stretching for 300 cycles at the strain of 50% (Figure 6b). Compared with a previously reported stretchable fiber-shaped lithium-ion battery on an elastic polymer substrate,[14,15] use of the springlike fiber electrodes without substrates, resulted in reduction of the volume and the weight of the battery by approximately 400% and 300%, respectively; the linear specific capacity was enhanced by 600%.

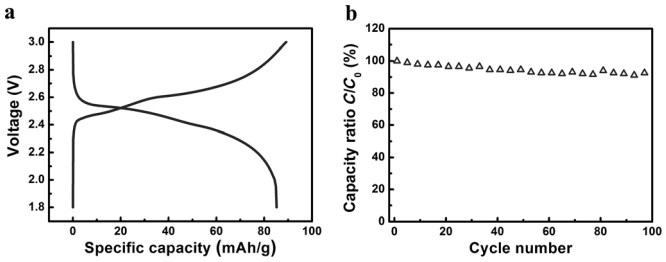

Figure 5. Electrochemical performance of a fiber-shaped lithium-ion battery made from the hybrid fiber. a) Charge and discharge profiles of the lithium-ion battery at a 0.1 mA cm^{-1}. b) Cyclic performance of the battery. C_0 and C correspond to the specific capacities at the first and following cycles, respectively.

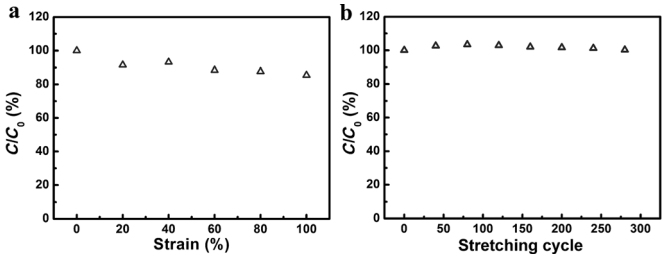

Figure 6. Evolution of specific capacitance with a) strain and b) stretch cycles.

In summary, flexible, elastic fiber-shaped supercapacitors and lithium-ion batteries were created based on freestanding springlike fiber electrodes. Both supercapacitors and lithium-ion batteries exhibited remarkable electrochemical properties that were resistant to bending and stretching deformations. This work further presents a general and effective route in developing highly stretchable electronic devices including solar cells and energy storage devices.

Experimental Section

Preparation of springlike fibers and hybrid fibers: Aligned CNT arrays were first synthesized by chemical vapor deposition by using previously reported methods.[20] CNT sheets with a width of ca. 1 cm were then drawn out of the aligned CNT array, followed by twisting into CNT fibers at a rotation speed of 1000 rpm. CNT fibers were placed in parallel with one end fixed onto a motor and the other fixed onto a paper slip, and then the motor steadily rotated at a speed of 700 rpm to produce the desired springlike fiber (20 cm of CNT fibers can produce ca. 5 cm of springlike fiber). During the twisting process, the paper slip was moved toward the motor to keep the fibers stretched and horizontal.

LMO particles were synthesized by a hydrothermal method. In a typical process, 0.377 g LiOH and 1.23 g γ-MnO_2 were first dissolved in 40 mL H_2O, followed by addition of 0.2 g glucose and 40 mL H_2O. The resulting mixture reacted at 200 °C for 24 h, followed by drying at 120 °C for 24 h. LTO particles were synthesized by using a solid-state method. 0.25 g TiO_2 and 0.1 g Li_2CO_3 were mixed and heated at 800 °C for 24 h, followed by ball-milling treatment for 20 h. To prepare the CNT/LTO and CNT/LMO hybrid fibers, either LMO or LTO nanoparticles were dispersed in *N*,*N*-dimethylformamide to prepare LMO and LTO suspensions with concentration of 5 mg mL^{-1}. Then the CNT sheets were immersed into suspensions and rolled into a hybrid fiber at a speed of 1000 rpm. Then ten CNT/LTO fibers and CNT/LMO fibers were twisted together at a speed of 700 rpm.

Fabrication of fiber-shaped supercapacitors and lithium-ion batteries: The gel electrolyte was prepared by dissolving 0.67 g polyvinyl alcohol (PVA) in 6.04 g deionized water at 90 °C for 5 h, followed by addition of 0.67 g H_3PO_4. Two springlike fibers were coated with the gel electrolyte and placed in parallel to produce a symmetric fiber-shaped supercapacitor. The gel electrolyte for lithium ion battery was prepared by dissolving 0.35 g poly(ethylene oxide) (PEO; $M_w \approx 600000$), 0.35 g succinonitrile, and 0.30 g lithium bis(trifluoromethane) sulfonimide (LiTFSI) in a mixture of methylene chloride and acetone (40:1, w/w), followed by stirring for 5 h at room temperature. The half-cells were assembled from the springlike fiber as electrode and the lithium wire as the counterelectrode. To assemble a full fiber-shaped battery, the springlike fiber anode and cathode were first coated with the gel electrolyte, and then twisted and encased in a heat-shrinkable tube. The springlike fibers were connected to copper wires by silver glue for the electrochemical analysis.

Characterization: The weight of the springlike fiber, and hybrid springlike fiber were measured by using a microbalance (Sartarious SE2). The structures were characterized by scanning electron microscope (Hitachi FE-SEM S-4800 operated at 1 kV) and X-ray diffraction (XRD, Bruker AXS D8). The weight contents of LTO and LMO in hybrid springlike fibers were determined by thermogravimetric analysis. Galvanostatic charge–discharge measurements were conducted at an ARBIN electrochemical workstation (MSTAT-5V/10mA/16Ch). The cyclic voltammetry was made by an electrochemical workstation (CHI 660D). The mechanical measurements were performed at table-top universal testing instrument (HY-0350). The photograph was taken by a camera (Nikon, J1).

Calculation: The volumetric specific capacitance (C_v) of the supercapacitor was calculated from the equation of $C_v = 2 \times I \times t/(v \times U)$, where I, t, v, and U correspond to the discharge current, discharge time, the fiber electrode volume and potential window, respectively. The volume (v) of the fiber electrode was calculated by multiplying the cross-sectional area and length. For instance, for a typical fiber electrode with length of 1 cm and diameter of 65 μm, the volume was determined as 3.32×10^{-5} cm^3. The gravimetric specific capacitance (C_m) was derived from the equation: $C_m = 2 \times I \times t/(m \times U)$. Here m corresponds to the mass of the springlike fiber electrode. It was calculated by multiplying the linear density and fiber length, typically 0.033 mg for a springlike fiber with a length of 1 cm. For the lithium-ion batteries, the specific capacity (C_m) was calculated from the equation of $C = (I \times t)/m$, where I, t, and m represent the discharge current, discharge time, and weight of the CNT/LTO fiber electrode, respectively. For a CNT/LTO fiber electrode with a length of 1 cm, the weight was 0.094 mg.

Received: September 23, 2014
Published online: October 30, 2014

Keywords: carbon nanotubes · flexible devices · lithium-ion batteries · nanoparticles · supercapacitors

[1] B. Y. Ahn, E. B. Duoss, M. J. Motala, X. Y. Guo, S. I. Park, Y. J. Xiong, J. Yoon, R. G. Nuzzo, J. A. Rogers, J. A. Lewis, *Science* **2009**, *323*, 1590 – 1593.
[2] K. Y. Chun, Y. Oh, J. Rho, J. H. Ahn, Y. J. Kim, H. R. Choi, S. Baik, *Nat. Nanotechnol.* **2010**, *5*, 853 – 857.
[3] G. S. Jeong, D. H. Baek, H. C. Jung, J. H. Song, J. H. Moon, S. W. Hong, I. Y. Kim, S. H. Lee, *Nat. Commun.* **2012**, *3*, 977.
[4] Y. Kim, J. Zhu, B. Yeom, M. Di Prima, X. L. Su, J. G. Kim, S. J. Yoo, C. Uher, N. A. Kotov, *Nature* **2013**, *500*, 59 – 63.
[5] C. Pang, C. Lee, K. Y. Suh, *J. Appl. Polym. Sci.* **2013**, *130*, 1429 – 1441.
[6] G. Park, H. J. Chung, K. Kim, S. A. Lim, J. Kim, Y. S. Kim, Y. Liu, W. H. Yeo, R. H. Kim, S. S. Kim, J. S. Kim, Y. H. Jung, T. I. Kim, C. Yee, J. A. Rogers, K. M. Lee, *Adv. Healthcare Mater.* **2014**, *3*, 515 – 525.
[7] Y. Wang, R. Yang, Z. W. Shi, L. C. Zhang, D. X. Shi, E. Wang, G. Y. Zhang, *ACS Nano* **2011**, *5*, 3645 – 3650.
[8] W. Zeng, L. Shu, Q. Li, S. Chen, F. Wang, X. M. Tao, *Adv. Mater.* **2014**, DOI: 10.1002/adma.201400633.
[9] M. L. Hammock, A. Chortos, B. C. K. Tee, J. B. H. Tok, Z. A. Bao, *Adv. Mater.* **2013**, *25*, 5997 – 6037.
[10] M. Park, J. Im, M. Shin, Y. Min, J. Park, H. Cho, S. Park, M. B. Shim, S. Jeon, D. Y. Chung, J. Bae, J. Park, U. Jeong, K. Kim, *Nat. Nanotechnol.* **2012**, *7*, 803 – 809.
[11] L. B. Hu, M. Pasta, F. La Mantia, L. F. Cui, S. Jeong, H. D. Deshazer, J. W. Choi, S. M. Han, Y. Cui, *Nano Lett.* **2010**, *10*, 708 – 714.
[12] K. H. Choi, S. J. Cho, S. H. Kim, Y. H. Kwon, J. Y. Kim, S. Y. Lee, *Adv. Funct. Mater.* **2014**, *24*, 44 – 52.
[13] H. Gwon, H. S. Kim, K. U. Lee, D. H. Seo, Y. C. Park, Y. S. Lee, B. T. Ahn, K. Kang, *Energy Environ. Sci.* **2011**, *4*, 1277 – 1283.
[14] Y. Zhang, W. Bai, J. Ren, W. Weng, H. Lin, Z. Zhang, H. Peng, *J. Mater. Chem. A* **2014**, *2*, 11054 – 11059.
[15] J. Ren, Y. Zhang, W. Bai, X. Chen, Z. Zhang, X. Fang, W. Weng, Y. Wang, H. Peng, *Angew. Chem. Int. Ed.* **2014**, *53*, 7864 – 7869; *Angew. Chem. Int. Ed.* **2014**, *126*, 7998 – 8003.
[16] Z. Yang, J. Deng, X. Chen, J. Ren, H. Peng, *Angew. Chem. Int. Ed.* **2013**, *52*, 13453 – 13457; *Angew. Chem.* **2013**, *125*, 13695 – 13699.
[17] S. Xu, Y. Zhang, J. Cho, J. Lee, X. Huang, L. Jia, J. A. Fan, Y. Su, J. Su, H. Zhang, *Nat. Commun.* **2013**, *4*, 1543.
[18] X. Li, T. L. Gu, B. Q. Wei, *Nano Lett.* **2012**, *12*, 6366 – 6371.
[19] C. Zhao, C. Wang, Z. Yue, K. Shu, G. G. Wallace, *ACS Appl. Mater. Interfaces* **2013**, *5*, 9008 – 9014.
[20] T. Chen, L. Qiu, Z. Yang, Z. Cai, J. Ren, H. Li, H. Lin, X. Sun, H. Peng, *Angew. Chem. Int. Ed.* **2012**, *51*, 11977 – 11980; *Angew. Chem.* **2012**, *124*, 12143 – 12146.
[21] M. Zhang, K. R. Atkinson, R. H. Baughman, *Science* **2004**, *306*, 1358 – 1361.
[22] Y. Shang, X. He, Y. Li, L. Zhang, Z. Li, C. Ji, E. Shi, P. Li, K. Zhu, Q. Peng, C. Wang, X. Zhang, R. Wang, J. Wei, K. Wang, H. Zhu, D. Wu, A. Cao, *Adv. Mater.* **2012**, *24*, 2896 – 2900.
[23] Y. Shang, Y. Li, X. He, S. Du, L. Zhang, E. Shi, S. Wu, Z. Li, P. Li, J. Wei, K. Wang, H. Zhu, D. Wu, A. Cao, *ACS Nano* **2013**, *7*, 1446 – 1453.
[24] J. Ren, W. Bai, G. Guan, Y. Zhang, H. Peng, *Adv. Mater.* **2013**, *25*, 5965 – 5970.
[25] J. Ren, L. Li, C. Chen, X. Chen, Z. Cai, L. Qiu, Y. Wang, X. Zhu, H. Peng, *Adv. Mater.* **2013**, *25*, 1155 – 1159.
[26] Y. Fu, X. Cai, H. Wu, Z. Lv, S. Hou, M. Peng, X. Yu, D. Zou, *Adv. Mater.* **2012**, *24*, 5713 – 5718.
[27] C. J. Yu, C. Masarapu, J. P. Rong, B. Q. Wei, H. Q. Jiang, *Adv. Mater.* **2009**, *21*, 4793 – 4797.
[28] P. Xu, T. L. Gu, Z. Y. Cao, B. Q. Wei, J. Y. Yu, F. X. Li, J. H. Byun, W. N. Lu, Q. W. Li, T. W. Chou, *Adv. Energy Mater.* **2014**, *4*, 1300759.
[29] Z. Q. Niu, H. B. Dong, B. W. Zhu, J. Z. Li, H. H. Hng, W. Y. Zhou, X. D. Chen, S. S. Xie, *Adv. Mater.* **2013**, *25*, 1058 – 1064.
[30] Y. Gogotsi, P. Simon, *Science* **2012**, *335*, 167 – 167.
[31] L. Cheng, X.-L. Li, H.-J. Liu, H.-M. Xiong, P.-W. Zhang, Y.-Y. Xia, *J. Electrochem. Soc.* **2007**, *154*, A692 – A697.
[32] Y.-Y. Liang, S.-J. Bao, B.-L. He, W.-J. Zhou, H.-L. Li, *J. Electrochem. Soc.* **2005**, *152*, A2030 – A2034.
[33] X. Huang, M. Lin, Q. TON, X. Li, Y. Ruan, Y. Yang, *J. Power Sources* **2012**, *202*, 352 – 356.
[34] H. Xiang, X. Zhang, Q. Jin, C. Zhang, C. Chen, X. Ge, *J. Power Sources* **2008**, *183*, 355 – 360.
[35] Y. Yang, S. Jeong, L. B. Hu, H. Wu, S. W. Lee, Y. Cui, *Proc. Natl. Acad. Sci. USA* **2011**, *108*, 13013 – 13018.

